

Presented at the 21<sup>st</sup> International Symposium on Acoustical Imaging, Laguna Beach, CA, March 1994. Published in *Acoustical Imaging, Vol. 21*, Joie P. Jones, Ed., Plenum Press: New York, pp. 31–38, 1995.

## A COMPARISON OF THE TRANSIENT PROPAGATION PROPERTIES OF GAUSSIAN AND BESSEL WAVES

John P. Powers; LT William Reid, USN; LCOL John G. Upton, USMC;  
and Ray Van de Veire

Naval Postgraduate School  
Department of Electrical and Computer Engineering, Code EC/Po  
833 Dyer Road, Room 437  
Monterey CA 93943-5121

### INTRODUCTION

Low-diffraction waves [1–5] have become of interest in ultrasound systems because of their longer depth of field for use in imaging and pulse-echo applications. Continuous-wave (CW) Bessel waves of infinite extent suffer no diffraction spreading [6–9]. Continuous spatially truncated Bessel waves also have less spreading than CW spatially truncated Gaussian waves. Here we use a computer-based simulation to investigate the propagation properties of *pulsed* Gaussian and Bessel waves with circularly finite extent. If the width of the Gaussian or Bessel wave is  $a$  and the diameter of the circle that truncates the wave is  $d$ , the ratio of  $d/a$  determines the propagation properties of the pulsed wave. Our propagation simulation uses fast Fourier spatial transforms to rapidly calculate the spatial impulse response wave,  $h(x, y, z, t)$ , at a location  $z$  in front of the source. The complete temporal response can be found by convolving the impulse response  $h(x, y, z, t)$  with the time excitation waveform  $T(t)$ . The predicted propagation patterns are presented to compare the behavior of the Gaussian and Bessel waves. For small ratios of  $d/a$ , the Gaussian and Bessel excitations can be made quite similar and the resulting diffraction patterns are also nearly the same. For large values of  $d/a$ , it is more difficult for the source functions to mimic each other and the wave patterns are quite different. In particular, in this regime of operation, the Bessel waves shows significant sidelobes, as the Bessel wave begins to have both positive and negative excitations. In the Gaussian wave, these sidelobes are absent, due to the smooth continuous nature of the Gaussian spatial excitation.

Figure 1 shows the geometry of the problem. The source is assumed to be located in a planar rigidly baffled region shown at the bottom of the figure. The normal velocity of the source is assumed to be known; we want to find the excited wave at the observation point  $(x, y, z)$  (or in the entire parallel plane located a distance  $z$  away from the source

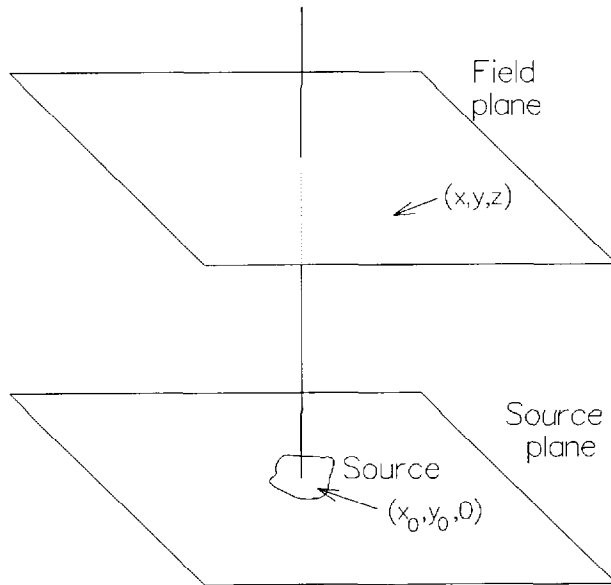


Figure 1: Geometry of source and receiving plane.

plane) as a function of time. The medium is assumed to be linear and homogeneous and has a velocity of 1500 m/s (i.e., that of water).

## REVIEW OF PROPAGATION SIMULATION TECHNIQUE

The propagation simulation technique [10, 11] is based on linear systems theory. We assume that the medium is lossless, linear, and homogeneous and that the source is surrounded by a rigid baffle. The first set of assumptions assures that propagation is a linear operation. The velocity of the source is assumed to be separable in space and time and is given by  $v(x_0, y_0, 0, t) = s(x, y)T(t)$ .

Figure 2 shows the block diagram approach to modeling propagation. In part (a) of the figure, we apply a point source spatial excitation with a temporal impulse,  $\delta(x, y)\delta(t)$ . By definition the resulting wave at the observation point is the *impulse response* of the propagation operation. Mathematically, this response is also the Green's function of the problem,  $g(x, y, z, t)$ . The Green's function for propagation into the half-space from a rigid baffle is known to be  $g(x, y, z, t) = \delta(ct - R)/2\pi R$  where  $R = \sqrt{x^2 + y^2 + z^2}$ .

When the propagation operation is excited by a temporal impulse with an arbitrary spatial excitation,  $s(x, y)\delta(t)$ , as shown in part (b) of Figure 2, linear systems theory predicts that the result,  $h(x, y, z, t)$ , is the spatial convolution of the impulse response,  $g(x, y, z, t)$ , with the spatial portion of the excitation,  $s(x, y)$ , or

$$h(x, y, z, t) = s(x, y) \underset{x}{*} \underset{y}{*} \delta(t). \quad (1)$$

Following the literature, we will call this result the *spatial impulse response* (i.e., the response to an arbitrary spatial excitation with a temporal impulse).

Finally, when the propagation operation is initiated by an arbitrary, separable function of space and time,  $s(x, y)T(t)$ , linear systems theory predicts that the result,  $\phi(x, y, z, t)$ , will be the temporal convolution of  $T(t)$  with the spatial impulse response,  $h(x, y, z, t)$ , or

$$\phi(x, y, z, t) = T(t) \underset{t}{*} h(x, y, z, t) = s(x, y)T(t) \underset{x}{*} \underset{y}{*} \underset{t}{*} g(x, y, z, t). \quad (2)$$

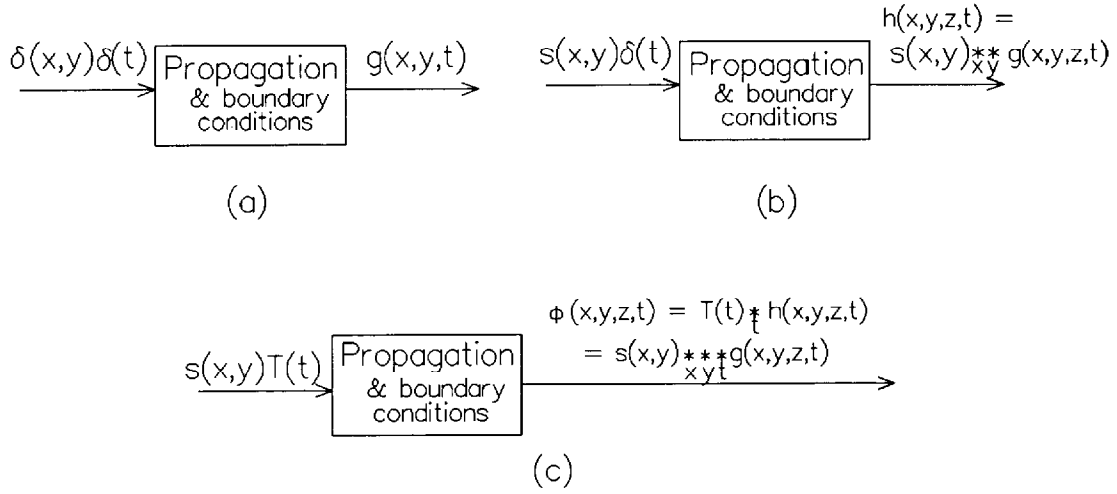


Figure 2: Block diagram explanation of propagation model. (a) Impulse response, (b) spatial impulse response, and (c) general to modeling the propagation.

The prospect of computing the triple convolution of Eq. 2 is daunting. Instead, we prefer to enter into the spatial transform domain in order to represent the double spatial convolutions as a multiplication. The two-dimensional spatial transform  $\tilde{a}(f_x, f_y)$  of a function  $a(x, y)$  is defined by

$$\tilde{a}(f_x, f_y) = \mathcal{F}\{a(x, y)\} = \int_{-\infty}^{\infty} \int_{-\infty}^{\infty} a(x, y) e^{+j2\pi(f_x x + f_y y)} dx dy. \quad (3)$$

The inverse two-dimensional spatial transform is

$$a(x, y) = \mathcal{F}^{-1}\{\tilde{a}(f_x, f_y)\} = \int_{-\infty}^{\infty} \int_{-\infty}^{\infty} \tilde{a}(f_x, f_y) e^{-j2\pi(f_x x + f_y y)} df_x df_y. \quad (4)$$

Taking the two-dimensional spatial transform of Eq. 2 gives

$$\tilde{\phi}(f_x, f_y, z, t) = T(t)_t^* [\tilde{s}(f_x, f_y) \tilde{g}(f_x, f_y, z, t)], \quad (5)$$

and taking the inverse transform provides

$$\phi(x, y, z, t) = T(t)_t^* \mathcal{F}^{-1}\{\tilde{s}(f_x, f_y) \tilde{g}(f_x, f_y, z, t)\}. \quad (6)$$

The transform of the propagation impulse response,  $\tilde{g}$ , is known as the *transfer function* of propagation. For the rigid baffle and propagation into the half-space of lossless media, this transfer function is known [10] to be

$$\tilde{g}(f_x, f_y, z, t) = J_0(\rho\sqrt{c^2 t^2 - z^2}) H(ct - z) \quad (7)$$

where  $\rho = \sqrt{f_x^2 + f_y^2}$  and  $H(\cdot)$  is the Heaviside step function. From this function we can picture propagation as a time-varying spatial filter that begins as an all-pass spatial filter and then increasingly becomes a low-pass spatial filter.

The method for simulating propagation, then, is

1. Find the two-dimensional Fourier transform of  $s(x, y)$ .
2. For each desired value of  $z$  and  $t$ , multiply the result with  $\tilde{g}(f_x, f_y, z, t)$  as expressed in Eq. 7.

3. Take the inverse two-dimensional inverse transform of the product to find the spatial impulse response,  $h(x, y, z, t)$ .
4. If desired, find the output for various  $T(t)$  by convolving  $T(t)$  with  $h(x, y, z, t)$ .
5. If desired, find the wave pressure  $p(x, y, x, t)$  from

$$p(x, y, z, t) = \rho_0 \frac{\partial \phi}{\partial t}, \quad (8)$$

where  $\rho_0$  is the density of the medium.

This simulation technique has been implemented in Fortran [12] and in MATLAB [13–15]. The following studies were produced with the MATLAB models.

## NUMERICAL SIMULATIONS

We now turn our attention to the simulation of the Gaussian and Bessel excitations. The equation for a symmetric Gaussian excitation that is truncated by a circle is

$$s_G(r; \sigma, d) = \begin{cases} e^{-r^2/\sigma^2} & \text{if } r < d/2 \\ 0 & \text{if } r \geq d/2 \end{cases} \quad (9)$$

where  $r$  is the radial distance from the  $z$  axis,  $\sigma$  is the “radius” of the curve at the  $1/e$ -amplitude points, and  $d$  is the diameter of the truncation circle. (In our simulations,  $d = 51$  samples; the sample points are located 2.5 mm apart [14,15].)

Similarly, the equation for the Bessel excitation is

$$s_B(r; a, d) = \begin{cases} J_0(ar) & \text{if } r < d/2 \\ 0 & \text{if } r \geq d/2 \end{cases} \quad (10)$$

where  $a$  is a scaling factor that controls the width of the Bessel function.

In our simulation, we chose to make the values of the spatial excitation functions equal at  $r = 0$  and at the half-maximum points (i.e., at the radius where each function is equal to one-half of its maximum value). For the chosen functions this relates  $a$  to  $\sigma$  by  $a = 1.291943/\sigma$ ; we will refer only to the value of  $\sigma$  from this point on. Figure 3 shows a cross-section of the Gaussian and Bessel excitations for  $\sigma = 2$  (i.e., narrow waves within the truncation circle). The Gaussian smoothly diminishes while the Bessel wave undergoes its oscillatory behavior before being truncated.

Figures 4 and 5 show perspective views of these spatial excitation functions for  $\sigma = 2$  and  $\sigma = 16$ , respectively. For  $\sigma = 16$ , the waves are appreciably wider within the truncation circle and closely resemble each other, as seen in the cross-section representation of the right side of Figure 3.

The calculated outputs for these pairs of input functions are shown in Figures 6 and 7. The resultant wave,  $h(x, y, z, t)$ , in our simulation is a 128x128x64 data array. Only one value of  $y$  is chosen for the plot, that corresponding to the cross-section located at  $y = 0$  (i.e., we plot  $h(x, 0, z, t)$ ). The other 127 cross-sections are not plotted. For our results, we have chosen the location at  $z = 10$  cm and selected a time span of approximately 0.4 milliseconds. The time interval begins just before  $t = z/c$ , i.e., just before the first arrival of the wave at the observation plane. It is noted that we also calculated the fields for values of  $\sigma$  between the values of 2 and 16, but do not show the results in order to conserve space.

We observe from Figure 7 that the waves are very similar. Upon looking at Figure 5 and the right figure of Figure 3, we observe that the input spatial excitation functions

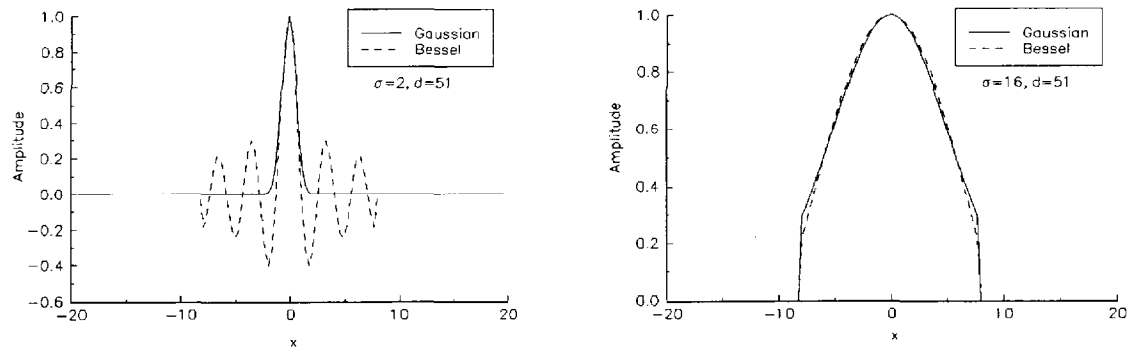


Figure 3: Cross-section of the input Gaussian and Bessel functions for (left)  $\sigma = 2$  and (right)  $\sigma = 16$ . The curves are matched at  $x = 0$  and at the half-maximum widths.

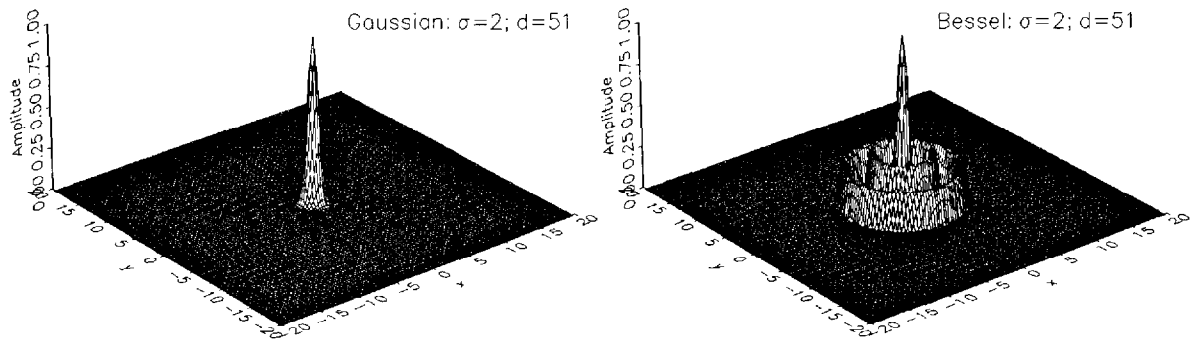


Figure 4: Perspective views of (left) the Gaussian spatial excitation function and (right) the Bessel excitation function for  $\sigma = 2$ .

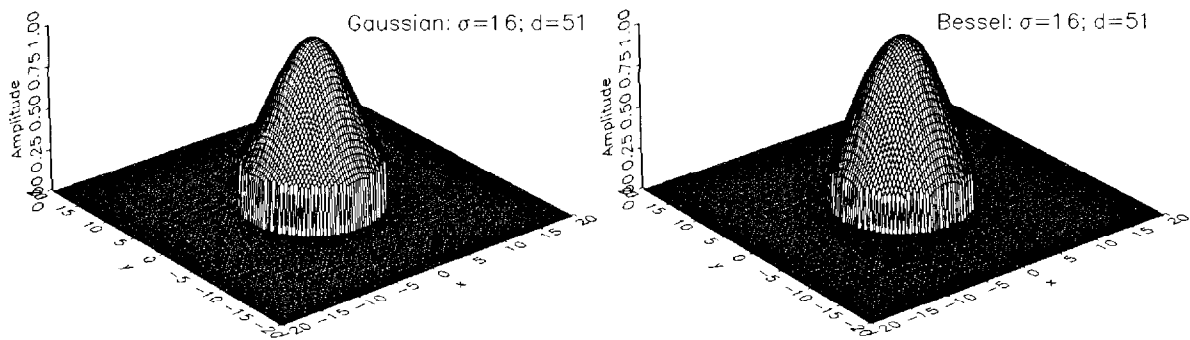


Figure 5: Perspective views of (left) the Gaussian spatial excitation function and (right) the Bessel excitation function for  $\sigma = 16$ .

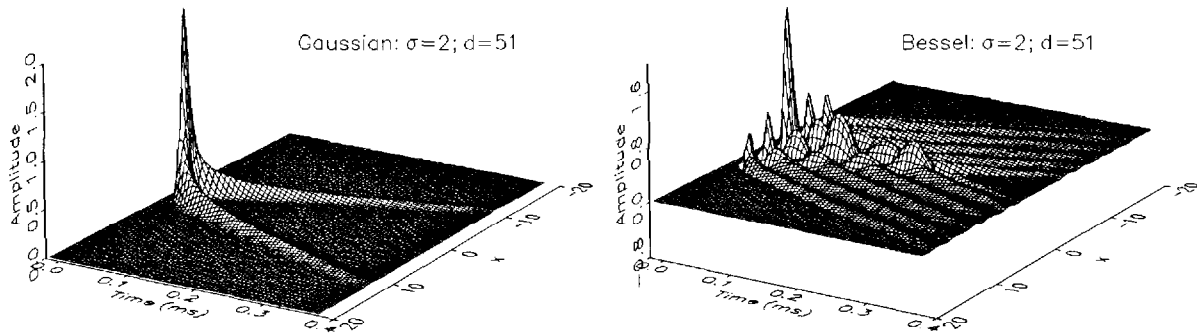


Figure 6: Perspective views of a cross-section,  $h(x, 0, 10 \text{ cm}, t)$ , for (a) the Gaussian function and (b) the Bessel function for  $\sigma = 2$ .

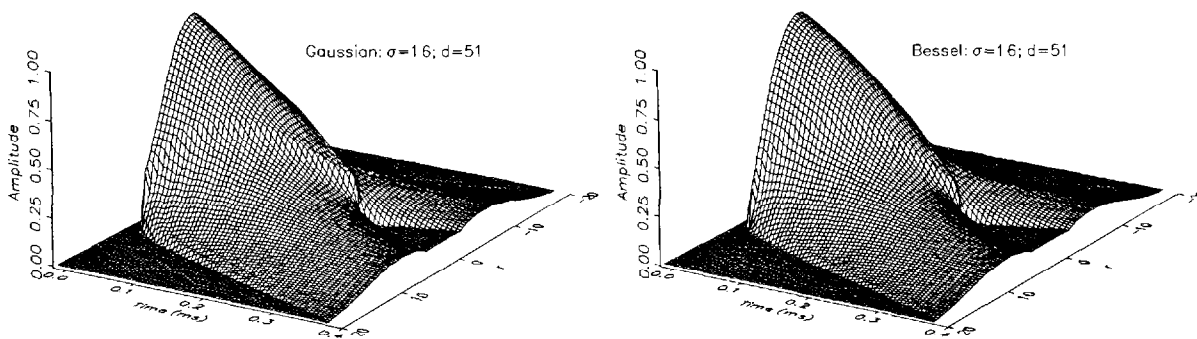


Figure 7: Perspective views of a cross-section,  $h(x, 0, 10 \text{ cm}, t)$ , for (a) the Gaussian function and (b) the Bessel function for  $\sigma = 16$ .

are almost the same for this (comparatively) large value of  $\sigma/d$ , hence it is not surprising that the spatial impulse responses are almost the same.

On the other hand, Figure 6 shows that the waves are quite dissimilar for small values of  $\sigma/d$ . This is intuitively expected after inspection of Figure 5 and the left side of Figure 3 since the excitations are quite different. In particular, we note from Figure 6 that the Bessel excitation produces fairly large sidelobes. (The negative lobes cannot be seen in this perspective view.) The depth of field along the  $t$ -axis centerline ( $x = 0$ ) is longer for the Bessel excitation, but also suffers from a nonuniform amplitude. The Gaussian excitation has the benefit of producing no sidelobes and falls abruptly along the time-axis centerline.

## SUMMARY

We have calculated the spatial impulse response of two spatially excited sources, a Gaussian spatial excitation and a Bessel spatial excitation. Both sources were spatially truncated by a circular aperture of diameter  $d$ . The excitation sources were equal-valued at their peaks and their half-maximum widths were equal. (This assumption related the Bessel scaling factor  $a$  to the Gaussian width parameter  $\sigma$ .) For large values of  $\sigma/d$ , the excitations and the spatial impulses were almost the same. For small values of  $\sigma/d$ , the excitations and the spatial impulse response differed widely. The Gaussian wave was characterized by the absence of any sidelobes and an abrupt decrease along the time-axis centerline. The Bessel-wave spatial impulse response exhibited both positive and negative sidelobes and a varying-amplitude wave along the time-axis centerline.

## ACKNOWLEDGEMENTS

This work was sponsored by the Direct-Funded Research Program of the Naval Postgraduate School with the cooperation of the Office of Naval Research.

## REFERENCES

- [1] J. Brittingham, "Focus wave modes in homogeneous Maxwell's equations: transverse electric mode," *J. Applied Physics*, vol. 54, pp. 1179-1189, 1983.
- [2] J. Lu and J. F. Greenleaf, "Ultrasonic nondiffracting transducer for medical imaging," *IEEE Trans. on Ultrasonics, Ferroelectrics, and Frequency Control*, vol. 37, no. 5, pp. 438-447, 1990.
- [3] J. Lu and J. F. Greenleaf, "Nondiffracting X waves — exact solutions to free-space scalar wave equation and their finite aperture realizations," *IEEE Trans. on Ultrasonics, Ferroelectrics, and Frequency Control*, vol. 39, no. 1, pp. 19-31, 1992.
- [4] J. Lu and J. F. Greenleaf, "Experimental verification of nondiffracting X waves," *IEEE Trans. on Ultrasonics, Ferroelectrics, and Frequency Control*, vol. 39, no. 3, pp. 441-446, 1992.
- [5] J. Lu and J. F. Greenleaf, "Sidelobe reduction for limited diffraction pulse-echo systems," *IEEE Trans. on Ultrasonics, Ferroelectrics, and Frequency Control*, vol. 40, no. 6, pp. 735-746, 1993.
- [6] J. Durnin, "Exact solutions for nondiffracting beams I. The scalar theory," *J. Optical Society of America A*, vol. 4, no. 4, pp. 651-654, 1987.
- [7] J. Durnin, J. Miceli, and J. Eberly, "Diffraction-free beams," *Physical Review Letters*, vol. 58, pp. 1499-1501, 1987.

- [8] J. Durnin, J. Miceli, and J. Eberly, "Comparison of Bessel and Gaussian beams," *Optics Letters*, vol. 13, pp. 79–80, 1988.
- [9] P. Kielczyński and W. Pajewski, "Acoustic field of Gaussian and Bessel transducers," *J. Acoustical Society of America*, vol. 94, no. 3, pp. 1719–1721, 1993.
- [10] D. Guyomar and J. Powers, "A Fourier approach to diffraction of pulsed ultrasonic waves in lossless media," *J. Acoustical Society of America*, vol. 82, no. 1, pp. 354–359, 1987.
- [11] D. Guyomar and J. P. Powers, "Boundary effects on transient radiation fields from vibrating surfaces," *J. Acoustical Society of America*, vol. 77, no. 3, pp. 907–915, 1985.
- [12] T. Merrill, *A transfer function approach to scalar wave propagation in lossy and lossless media*, Master's thesis, Naval Postgraduate School, Monterey, California, March 1987.
- [13] J. Upton, *Microcomputer simulation of a Fourier approach to optical wave propagation*, Master's thesis, Naval Postgraduate School, Monterey, California, March 1992.
- [14] W. R. Reid, *Microcomputer simulation of a Fourier approach to ultrasonic wave propagation*, Master's thesis, Naval Postgraduate School, Monterey, California, December 1992.
- [15] J. P. Powers, "Acoustic propagation modeling using MATLAB," Tech. Rep. NPS EC-93-104, Naval Postgraduate School, Monterey, California, September 1993.